

Color-center creation in LiF under irradiation with swift heavy ions: Dependence on energy loss and fluence

K. Schwartz,¹ C. Trautmann,^{1,*} A. S. El-Said,¹ R. Neumann,¹ M. Toulemonde,² and W. Knolle³

¹*Gesellschaft für Schwerionenforschung (GSI), Planckstrasse 1, 64291 Darmstadt, Germany*

²*CIRIL, Laboratoire commun CEA/CNRS, B.P. 5133, 14070 Caen-cedex 5, France*

³*Leibnitz Institut für Oberflächenmodifizierung (IOM), Permoserstrasse 15, 04318 Leipzig, Germany*

(Received 8 April 2004; published 4 November 2004)

Single crystals of LiF exposed to swift heavy ions respond by the creation of color centers and defect aggregates. We present a comprehensive study by means of optical absorption spectroscopy using various MeV-GeV ions from ⁴He to ²³⁸U and a broad range of fluences. In the single-track regime, the defect characteristics such as the F-center concentration as a function of fluence and energy loss are analyzed. At large fluences, track overlapping occurs and the damage process is dominated by the formation of complex F_n centers and defect aggregates. The evolution of F-center and defect clusters is discussed in terms of aggregation as well as recombination of electron and hole centers. Limited efficiency for defect creation with heavy ions is mainly ascribed to annihilation processes of electron and hole centers.

DOI: 10.1103/PhysRevB.70.184104

PACS number(s): 61.43.-j

I. INTRODUCTION

The study presented here is dedicated to defect creation in single crystals of lithium fluoride (LiF) irradiated with swift heavy ions in the MeV to GeV energy range. The basic damage process consists in the production of Frenkel pairs which finally transform into more complicated defect and defect clusters. In contrast to many insulators, LiF does not amorphize, even not when exposed to high doses. This property is characteristic for materials with strong ionic binding and directed orientation of the interatomic bonds, such as the alkali halides.¹

The very first damage study on LiF crystals exposed to heavy projectiles was published by Young, who revealed tracks of fission fragments by chemical etching.² Later, more detailed investigations by Perez *et al.*^{3,4} and Thévenard *et al.*⁵ focused on electron color centers created along the paths of mainly light ions. They demonstrated that the concentration of single defects is directly proportional to the stopping power of the projectiles. Balanzat *et al.* studied color center creation in LiF, NaCl, and KBr crystals at low temperatures,⁶ giving evidence that in alkali halides the exciton mechanism known from experiments with classical radiation sources is also responsible for ion-induced luminescence and color-center creation. More recently, experiments with a large number of different heavy ions and MeV-GeV energies showed the existence of threshold effects that are linked to swelling,⁷ formation of surface hillocks,^{8,9} sputtering,¹⁰ chemical track etching,¹¹ change of electron density,¹² and hole clusters.¹³ From a large data set obtained by various methods, it was concluded that tracks induced by heavy projectiles of large stopping power can be described by a core region (radius 1–2 nm) with complex defect aggregates,^{12,13} surrounded by a large zone of defects responsible for swelling.⁷ Furthermore, there is an extended track halo (radius 5–30 nm) with mainly simple color centers.^{12,14,15} This nonhomogeneous defect distribution is a consequence of the $1/r^2$ profile of the deposited energy (where r is the radial distance from the ion path).¹²

In alkali halides and alkaline earth halides, radiation creates, almost exclusively, damage in the halogen sublattice, whereas the alkali sublattice remains nearly intact. Under irradiation, the primary defects in LiF are Frenkel pairs consisting of neutral (F and H centers) or charged (α and I centers) color centers. The most dominant defects are F centers [an electron localized at a fluorine vacancy (v_a^+)] together with the complementary interstitial hole centers (H center), e.g., an anion molecule consisting of a neutral X^0 and a charged X^- halogen atom (X_2^-) at a regular anion lattice position.^{16,17} In ionic crystals, defect formation processes are governed by the high mobility of the primary hole centers, which is, in general, orders of magnitude larger than that of F centers. At low temperatures, the defect formation under conventional irradiation is limited because electron and hole centers can not be separated spatially and thus easily annihilate by recombination. At room temperature, diffusion in particular of hole centers plays a dominant role, and H centers are transformed to stable V_3 centers of type X_3^- .^{18,19}

Damage creation becomes more complicated at high irradiation doses, where the concentration of single defects becomes large, and neighboring defects can easily coagulate forming more complex defects. In the case of electron color centers, these are point defects (e.g., F_2^- , F_3^- , and F_4^- -centers) and F-center aggregates such as nF centers (where n denotes the number of F centers in the cluster) and Li colloids. For energetic ion beams, aggregation processes occur in each single track, but they also take place when neighboring tracks overlap. In preirradiated areas, electron color centers (F, F_n, F_n^+, F_n^-) may interact with charge carriers [electrons (e^-) and holes (e^+)] or lattice vacancies.^{20–25} Such processes have different kinetics, being fast for charge carriers and slow for vacancy diffusion. In addition, they depend on several parameters such as the irradiation temperature, fluence, and energy loss. Diffusion plays not only a crucial role for defect aggregation but also for recombination of electron and hole centers.

The aim of this study is to identify various stages of aggregation and recombination processes of color centers when

LiF crystals are exposed to heavy ions of different beam parameters. We concentrate on electron color centers because they are easily accessible by means of optical absorption spectroscopy in the UV and visible spectral region, whereas V_3 hole centers absorb in the vacuum ultraviolet region.^{13,18,19} Ion projectiles between helium and uranium of MeV to GeV energy were used covering a wide range of fluence and energy loss values. The large data set allows us to make a detailed analysis of color-center creation for individual tracks at low fluences and for overlapping tracks at high fluences. We also evaluate the efficiency of color-center creation for different ion beams and compare this to irradiations with ^{60}Co γ rays.

II. EXPERIMENTAL

A. Irradiation

Samples were obtained from a single-crystal LiF block grown from a melt in an inert atmosphere (Korth Kristalle, Germany). Thin platelets were cleaved from the crystal block along one of the (100) planes with size $\sim 10 \times 10 \text{ mm}^2$ and thickness between 0.1 and 1 mm. Ion irradiations were performed either at the UNILAC linear accelerator of GSI (Darmstadt, Germany) or at the GANIL accelerator (Caen, France). The energy of the various projectiles (from C up to U) was between 30 and 2640 MeV with a beam flux of the order $10^9 \text{ ions s}^{-1} \text{ cm}^{-2}$ for light ions and $4 \times 10^8 \text{ ions s}^{-1} \text{ cm}^{-2}$ for heavy ions. Additional irradiations with 5-MeV α particles were carried out at a smaller 7 MV Van-de-Graaff accelerator (Frankfurt/M, Germany). All samples were irradiated at room temperature and at normal incidence, with fluences between 10^9 and $10^{15} \text{ ions/cm}^2$. The ion range was in all cases less than the sample thickness, i.e., the beam was stopped in the crystals. The interaction of the energetic projectiles with the target is characterized by almost pure electronic excitations while elastic collisions are dominant only at the stopping end of the ion path (less than $1 \mu\text{m}$). Since the optical spectroscopy data results from defects along the entire ion path, we use the mean energy loss (total energy divided by ion range) which varies from 0.27 for α particle up to 26.9 keV/nm for U ion. Table I lists the beam parameters of different irradiation experiments.

For comparative studies in the low-dose regime, some LiF crystals were exposed to γ rays with a dose rate $\sim 2 \text{ Gy/s}$ using the PANORAMA ^{60}Co source at the IOM (Leipzig, Germany).

B. Fluence and dose measurements

The dose of the γ irradiation was determined by graphite calorimetry with an accuracy of about $\pm 10\%$. In the case of ion beams, the fluence accumulation during irradiation was measured by recording the signal from a secondary-electron-emitting Al-foil detector placed in front of the samples. The electron signal was calibrated to the ion current via a Faraday cup leading to an accuracy of about 20%. We additionally crosschecked the fluence offline by track etching of polycarbonate foils²⁷ irradiated under identical beam conditions. The homogeneity of the defocused ion beam within an area of

TABLE I. Irradiation parameters: The energy loss averaged along the entire ion path is calculated from the total energy divided by the ion range (E/R). The range values are estimated with the TRIM 92 code (Ref. 26).

Ion species	Energy (MeV)	Range (μm)	E/R (keV/nm)	fluence (ions/cm ²)
^4He	5	19	0.27	$10^{11} - 10^{15}$
^{12}C	137	255	0.5	$10^9 - 10^{13}$
^{22}Ne	31	12	2.5	$5 \times 10^{11} - 3 \times 10^{13}$
^{36}S	410	136	3.0	$10^9 - 10^{13}$
^{58}Ni	170	21	7.8	$10^9 - 2 \times 10^{12}$
	640	92	7.0	
^{64}Zn	710	93	7.7	$10^9 - 10^{12}$
^{82}Se	910	101	9.0	$10^9 - 10^{10}$
^{96}Mo	400	35	11.6	$5 \times 10^{10} - 10^{12}$
	300	20	15.0	
^{129}Xe	1400	88	16	$10^9 - 10^{12}$
^{197}Au	2190	93	23.5	$10^9 - 10^{12}$
^{208}Pb	830	38	21.8	$10^9 - 10^{12}$
	2310	93	24.8	
^{209}Bi	1170	51	22.9	$10^9 - 10^{12}$
	2320	93	24.9	
^{238}U	1400	57	24.6	$10^9 - 10^{12}$
	2640	98	26.9	

about $4 \times 4 \text{ cm}^2$ was of the order 10–20%. For some selected samples (2310 MeV Pb), the precision of the fluence determination was better ($\sim 8\%$) because the polymer test foil was mounted directly in front of the given crystal.

For a comparison of radiation effects between different ions, and between ions and γ rays, the applied fluence was transformed into a mean dose D by using the following formula:

$$D = 1.6 \times 10^{-10} \times E \times \Phi / (\rho \times R), \quad (1)$$

where D is given in Gy, E is the total ion energy in MeV, Φ denotes the fluence in ions/cm², $\rho = 2.635 \text{ g/cm}^3$ is the mass density of LiF, and R is the range in cm.

C. Optical absorption spectroscopy

Optical absorption measurements were performed with a double-beam spectrometer (ATI Unicam UV4) in the spectral range of 200–700 nm. The most significant electron defects are F centers and F_2 centers (two localized electrons at two neighboring anion vacancies) with absorption maxima at ~ 250 and ~ 445 nm, respectively. The total number of F and F_2 centers within a unit area of the sample (areal density) was determined by applying the Smakula-Dexter formula with respective oscillator strengths of $f_F = 0.6$ and $f_{\text{F}_2} = 0.3$.⁴

TABLE II. Absorption bands of various electron color centers and Li colloids due to high dose irradiations according to Refs. 3, 25, and 28. The parameters λ_{\max} and E_{\max} denote, respectively, the wavelength and energy at band maximum. Some of the defect centers have two absorption bands according to specific structural positions. The two colloid bands correspond to different colloid sizes.

Center	F	F ⁻	F ₂	F ₂ ⁺	F ₃	F ₃ ⁺	F ₄	Colloid				
λ_{\max} (nm)	250	950	445	625	317	377	660	790	518	540	450	530
E_{\max} (eV)	4.96	1.31	2.79	1.98	3.91	3.29	1.88	1.57	2.39	2.30	2.76	2.34

$$n_F = 9.48 \times 10^{15} \times D_{\text{opt}} \quad \text{and} \quad n_{F_2} = 4.42 \times 10^{15} \times D_{\text{opt}}, \quad (2)$$

where n_F and n_{F_2} are given in cm^{-2} , and D_{opt} denotes the baseline-corrected optical density at the absorption maximum, assuming that the full width at half maximum (FWHM) of the band does not change.

The absorption measurement has an upper limit given by the maximum optical density of $D_{\text{opt}} \leq 4$, which corresponds to a total number of F centers of about $4 \times 10^{16} \text{ cm}^{-2}$. Minimum measurable concentrations are of the order of 10^{14} cm^{-2} ($D_{\text{opt}} \sim 0.01$).

For samples irradiated with higher fluences, the spectra become rather complicated because single defects aggregate to more complex F_n centers ($n=2,3,4$) with bands in the spectral region between 300 and 600 nm. Most of the absorption bands of these aggregate centers are known from experiments with various ionizing radiation sources (Table II).^{3,16,25,28-31} An exception are colloids, which are not definitively identified by optical spectroscopy due to the fact that LiF can not be colored additively.²⁵ Since the different bands in the 300–600 nm region strongly overlap, it is impossible to analyze individual contributions separately. At high fluences, we therefore determined the integrated absorption

$$A = \int_{300}^{600} D_{\text{opt}} d\lambda. \quad (3)$$

The oscillator strengths of the different F_n and $F_n^{+/-}$ centers are rather similar,^{20,25,31} thus A gives a useful approximation to compare the evolution of all complex electron color centers for different irradiations.

III. RESULTS

The optical spectrum of irradiated LiF is dominated by the strong F-center band at 250 nm and the F_2 -center band at 445 nm. The character of the spectra clearly depends on the applied ion fluence (Fig. 1). We therefore treat the low- and high-fluence regime separately. At low fluences the F-center concentration increases approximately linearly with fluence, whereas at high fluences saturation effects appear and the absorption bands become broader.

A. Low ion fluence

For irradiations at low fluences, the absorption band of the F and the F_2 center are well separated and can be analyzed

individually, except for some samples exposed to light ions where the F_2 -center absorbance was extremely weak and difficult to quantify [Fig. 1(a)]. We note that the low-fluences regime includes values around 10^{11} cm^{-2} for light projectiles (e.g., He), but a maximum of $\sim 5 \times 10^9 \text{ cm}^{-2}$ for the heavy ions.

For a quantitative comparison of the F-center creation induced by different ions, we analyzed the optical data according to Eq. (2) and determined the concentration N_F (cm^{-3}) by normalizing n_F by the ion range

$$N_F = n_F/R. \quad (4)$$

In order to discuss the F-center efficiency, we determine the total number of F centers per single ion track by

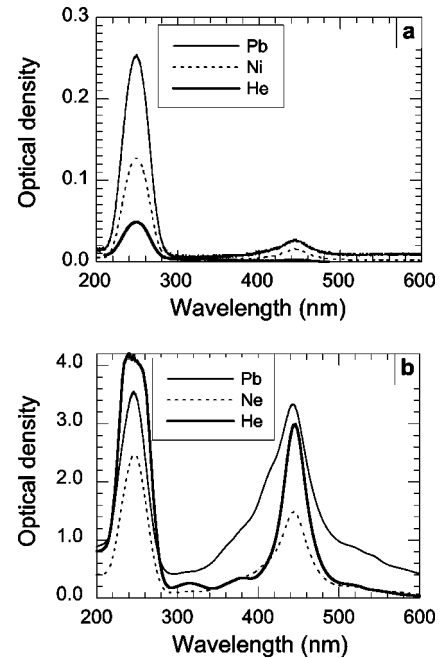


FIG. 1. Absorption spectra of LiF crystals irradiated with light, medium, and heavy ions of different fluence (and corresponding dose). (a) Low-fluence irradiation with 5-MeV He ions (10^{11} cm^{-2} , 18 kGy), 170-MeV Ni ions (10^9 cm^{-2} , 5 kGy), and 2310-MeV Pb ions (10^9 cm^{-2} , 15 kGy); the inset shows the F_2 -center bands at higher magnification. (b) High-fluence irradiation with 5-MeV He ions (10^{14} cm^{-2} , 16 MGy), 31-MeV Ne ions (10^{13} cm^{-2} , 15 MGy) and 830-MeV Pb ions ($1.2 \times 10^{12} \text{ cm}^{-2}$, 16 MGy).

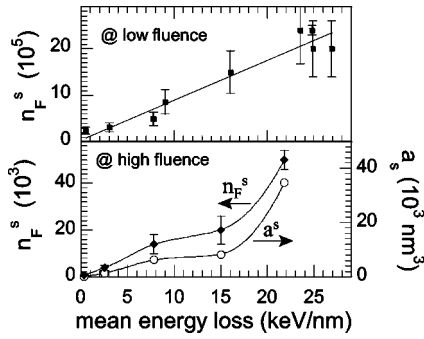


FIG. 2. Number of F centers n_F^s and defect clusters a^s per ion track [see Eq. (8)] as a function of mean energy loss: (a) low-fluence and (b) high-fluence regimes; (the lines are guides to the eye).

$$n_F^s = n_F \Phi. \quad (5)$$

Figure 2(a) shows the n_F^s data of various low-fluence irradiation experiments as a function of the mean energy loss, increasing steadily from a few 10^5 for light ions up to more than 2×10^6 for the heaviest projectiles.

The accuracy of the data is determined by the inhomogeneity of the ion irradiation and by the uncertainty of the absolute fluence. We estimate the following errors: 15% for n_F mainly due to the beam inhomogeneity, $\sim 20\%$ for N_F due to the additional range uncertainty, and a total error of $\sim 30\%$ for n_F^s .

As typically done for classical radiations, the efficiency for the creation of single F centers is deduced from the total energy deposition and the number n_F^s of stable F centers produced. Since in the low-fluence regime, the concentration of F centers is much larger than that of all F_n aggregates, the mean energy ΔE_F per F center (or more precisely per $F-V_3$ pair) is calculated by

$$\Delta E_F = E/n_F^s, \quad (6)$$

ΔE_F is ~ 500 eV for carbon ions and scatters around 1100 eV for all heavier projectiles, probably due to the large error given by the experimental uncertainties discussed above. In the experiment with 2310-MeV Pb ions, the precision was better ($\pm 8\%$) yielding an energy of $\Delta E_F = 960 \pm 80$ eV, which is more than twice as large as $\Delta E_F = 440 \pm 40$ eV for ^{60}Co γ rays or for the light C ions. As we will discuss later in more details, this lower efficiency is a direct indication for additional processes such as recombination of electron and hole centers and aggregation of single to more complex defects ($F \rightarrow F_n$ and $F \rightarrow nF$).

B. High ion fluence

With increasing fluences, the optical spectra become more complex as illustrated in Fig. 3 for a sample irradiated with 400-MeV Mo ions. Compared to low fluences, the following important effects appear: the overall absorption in the wavelength regime 300–600 nm around the F_2 band increases significantly, and the evolution of the F- and the F_2 -band intensities as a function of fluence are quite different (cf., 6×10^{11} and 1×10^{12} ions/cm 2 in Fig. 3). We note, e.g., that

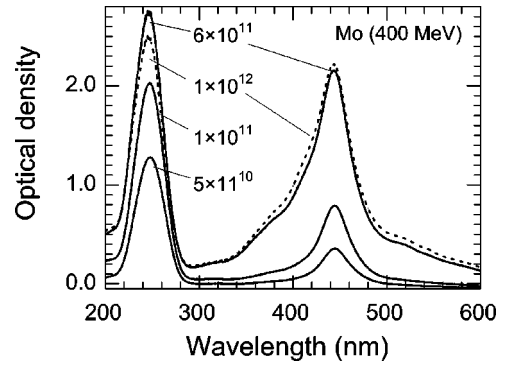


FIG. 3. Absorption spectra of LiF crystals irradiated with 400-MeV Mo ions. The different fluences are indicated in units of ions/cm 2 .

the F-center absorption decreases at highest fluence, whereas that of the F_n centers (300–600 nm) saturates.

For a quantitative comparison of defect formation of different ion species, the F-center bands are analyzed as a function of the dose (Fig. 4; due to saturated optical density, the two He data points at highest fluence were extrapolated from FWHM estimations). We selected the dose instead of fluence as parameter, because it takes into account the energy and range of the different ions [see Eq. (1)]. In the low-dose regime, N_F increases linearly with a similar initial slope for all projectiles, while above a few MGy, N_F follows a saturation curve. At highest dose, the Pb data surpass a maximum and then decrease, whereas the data of the light ions such as He and Ne exhibit a weak linear rise. It should be mentioned that a low-slope increase at high dose is also known from classical radiations using electrons, γ rays, or neutrons.^{20,32,33} Best fits to the N_F -versus-dose data can be obtained by an exponential law (in the case of He and Ne superimposed by a linear function):

$$N_F = N_0[1 - \exp(-\sigma_d \times D)], \quad (7)$$

where N_0 describes a saturation level and σ_d is related to the track cross section. Figure 4 clearly shows that N_0 is higher for lighter ions, indicating that for smaller deposited energy densities, the volume concentration of stable F centers is

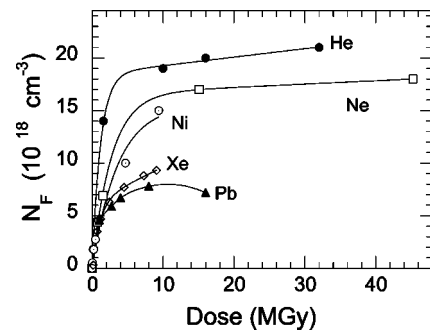


FIG. 4. Volume concentration of F centers as a function of applied dose. At 8 MGy, the corresponding fluence of the different ion species is 5×10^{13} (He, 5 MeV), 5.3×10^{12} (Ne, 31 MeV), 1.7×10^{12} (Ni, 170 MeV), 9×10^{11} (Xe, 300 MeV), and 6×10^{11} ions/cm 2 (Pb, 830 MeV).

TABLE III. Beam parameters and optical data of various irradiations at a dose of ~ 8 MGy close to the saturation regime (cf. Fig. 4). The concentration of single F centers is characterized by n_F and n_F^s analyzed according to Eqs. (2) and (5), respectively. Defect aggregates per track a^s are described by the integrated absorbance in the wavelength range 300–600 nm [Eq. (3)] divided by the fluence. The F-center track radius r_F was deduced from the evolution of N_F vs fluence by applying the Thévenard model [see section after Eq. (7)]. The parameter Φ_c denotes the critical fluence where 66% of the irradiated sample is modified [$1 - \exp(\sigma \times \Phi_c) = 0.66$].

Ion	^4He	^{22}Ne	^{58}Ni	^{129}Xe	^{208}Pb
E (MeV)	5	31	170	300	830
E/R (keV/nm)	0.3	2.5	7.8	15.0	21.8
Fluence (10^{12} cm $^{-2}$)	50	5.3	1.7	0.9	0.6
n_F (10^{16} cm $^{-2}$)	3.3	2	2.9	2.0	3
Radius r_F (nm)	2	4	14	16	18
n_F^s (10^3)	0.7	3.8	14	20	50
A_F (nm)	160	86	104	70	128
A (nm)	135	90	126	100	238
a^s (10^2 nm 3)	0.9	13	63	82	347
n_e^s (10^3)	1.9	12	48	77	240
ΔE_c (keV)	2.6	2.6	3.5	3.9	3.5
Φ_c (10^{12} cm $^{-2}$)	8	2	0.16	0.12	0.1

larger probably because primary recombination processes of electron and hole centers are less dominant.

The defect data of various irradiations close to the saturation regime ($D \sim 8$ MGy) is presented in Table III. We note that within 30% all ions induce approximately the same F center concentration of $n_F \sim 3 \times 10^{16}$ cm $^{-2}$. Thévenard *et al.* proposed an analysis of the absorption-versus-fluence data by using an exponential function similar to Eq. (7).²⁸ The dose D is replaced by the fluence Φ , and σ_d is substituted by σ representing the cross section of a cylindrical track in which the F centers are created. The F-center concentration in each track is supposed to be saturated and to have a homogeneous lateral distribution. Track overlapping occurs when the distance of two different ion impacts is smaller than the track diameter ($2 r_F$), leading to complex F_n centers via F-center aggregation. Applying this simplified model to our data, we deduce $\sigma = \pi(r_F)^2$, where r_F denotes the F-center track radius (track cylinder filled with F centers). The r_F values increase from ~ 2 nm for He ions to ~ 18 nm for Pb projectiles (see Table III). It is interesting to mention, that at a dose of $D \sim 8$ MGy, the mean distance between tracks [$d = 2(\pi\Phi)^{-1/2}$] is slightly smaller than r_F , indicating that the F-center-containing track zones already overlap.

Another interesting observation concerns the shape of the F-center band. At low fluences, the FWHM is $G \sim 37$ nm (0.76 eV), in agreement with literature.^{31,34} At higher fluences Γ increases; the effect is more pronounced for samples exposed to heavier ions of higher energy loss [Fig. 5(a)]. When subtracting two spectra of different fluences from each other, we directly see the asymmetric band broadening as illustrated in Fig. 5(b). Deconvolution of the peak identifies the shoulder as a new band with maximum at ~ 225 nm. A

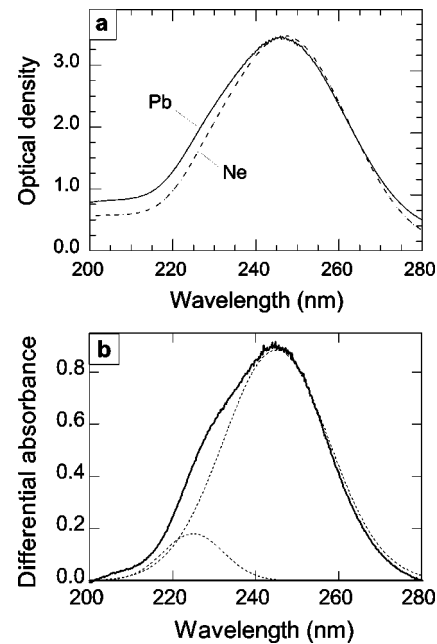


FIG. 5. Optical absorption spectra in the wavelength range around the F-center band: (a) Spectrum of sample irradiated with 31-MeV Ne ions (10^{13} cm $^{-2}$, 15 MGy) and with 830-MeV Pb ions (1.2×10^{12} cm $^{-2}$, 16 MGy). For better comparison, the data are normalized to equal band maximum. (b) differential spectrum ($\Phi_2 - \Phi_1$) of irradiation with 400-MeV Mo ions at $\Phi_1 = 5 \times 10^{10}$ and $\Phi_2 = 10^{12}$ ions/cm 2 . The dotted curves result from deconvolution.

defect band at this wavelength was observed by Delbecq and Pringsheim in LiF crystals irradiated with a high dose of x-rays. The band could reversibly be converted into F centers by illumination in the 225 nm absorption band and was thus assigned to specific nF-center clusters and not to large colloids.²⁹

Between 300 and 600 nm, the high-fluence spectra show a significant change as illustrated in Fig. 6 for samples irradiated with Ne and U ions, and for comparison with γ rays. In the latter case, the F_3 and F_4 bands appear rather well separated from the F_2 band, whereas ion beams induce an overall broadening of the entire region 350–500 nm region. The effect is stronger for higher fluences and for heavier projectiles.

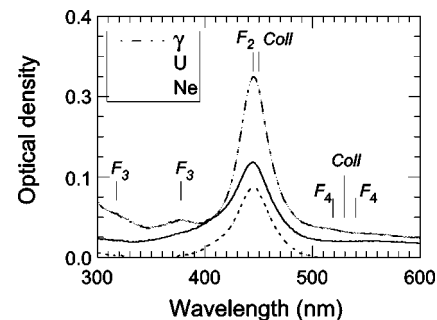


FIG. 6. Absorption spectra of samples irradiated with γ rays (275 kGy), 31-MeV Ne ions (750 kGy, 5×10^{11} cm $^{-2}$), and 1400-MeV U ions (150 kGy, 10^{10} cm $^{-2}$). The band positions of different color centers and colloids are indicated.

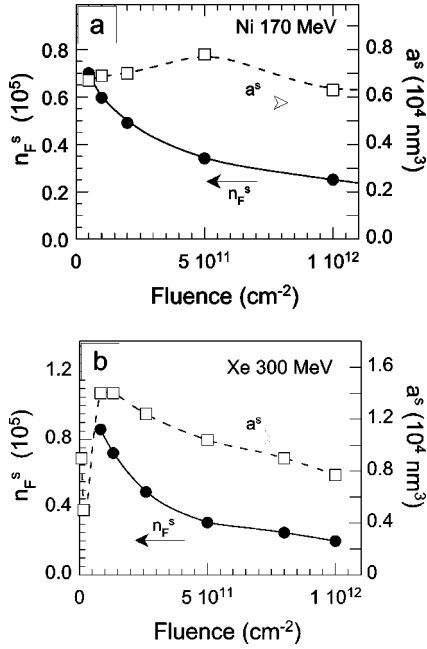


FIG. 7. Number of F centers (n_F^s) and defect clusters (a^s) per ion as a function of fluence for irradiations with (a) 170-MeV Ni, and (b) 300-MeV Xe ions. The lines are guides to the eye.

At high fluences, the large integral absorption of the complex defect shows us that the F_n concentration becomes comparable or even larger than that of single F centers. In order to analyze the number of defect aggregates per track, we define, in analogy to n_F^s , the integral absorption per ion in units of nm³ (Table III):

$$a^s = A/\Phi. \quad (8a)$$

The evolution of n_F^s and a^s as a function of the fluence is shown in Figs. 7(a) and 7(b). While n_F^s decreases steadily, a^s increases in the initial phase and then reaches a maximum at a certain fluence. For heavier particles, this maximum appears at a lower critical fluence than for light ions (e.g., at 5×10^{11} cm⁻² for Ni and $\sim 2 \times 10^{11}$ cm⁻² for Xe ions). Beyond this, a^s also decays in a similar way as n_F^s .

To compare quantitatively how the defect concentrations evolve for different ion species, we plot n_F , n_F^s , and a^s as a function of dose on a semilogarithmic scale [Figs. 8(a) and 8(b)]. For all ions, n_F first increases and then reaches (Ne) or surpasses a maximum (Pb) at about 10 MGy. In contrast to that, n_F^s decreases continuously in the entire dose regime. Similar to the data of Fig. 7, a^s exhibits an initial increase, then has a broad maximum at around 1.5 MGy for Pb ions and around 10 MGy for Ne ions and, and finally also decays. The dependence of a^s on the mean energy loss of the projectiles is shown in Fig. 2(b), following the same evolution as n_F^s . Note that at a given dose, a^s of Pb ions is more than two orders larger than for α particles (Table III).

In order to discuss the efficiency for defect creation at high fluence, the energy needed for a Frenkel pair cannot be calculated from Eq. (6), because the large number of complex defects a^s has to be included in the energy balance. We therefore estimated the concentration of all electron color

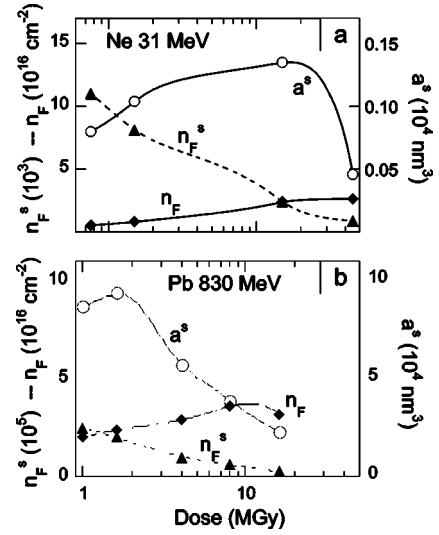


FIG. 8. Evolution of F-center concentration per track (n_F^s), of total F-center concentration (n_F), and of defect clusters per track (a^s) vs dose for irradiations with (a) 31-MeV Ne and (b) 830-MeV Pb ions. The lines are guides to the eye.

centers n_e by summing up single F centers (n_F) and complex F_n centers according to

$$n_e = n_F + 2n_F(A/A_F), \quad (8b)$$

where A is the integral absorption in the 300–600 nm spectral range as defined in Eq. (3), and A_F is the corresponding value for the F-center band from 210–290 nm. The factor two takes into account that the oscillator strength of F_2 and other F_n centers is about half as large as that of F centers.^{25,31} From n_e we can estimate the number of all electron centers per single track and the energy to create a Frenkel pair in the high-fluence regime

$$n_e^s = n_e/\Phi \quad \text{and} \quad \Delta E_e = E/n_e^s, \quad (8c)$$

From the values listed in Table III, we note that at high fluences, the efficiency does not strongly depend on the ion beam and is much smaller than at low fluences.

IV. DISCUSSION

Similar to classical radiation with γ rays, electrons, and neutrons, the irradiation with energetic ion projectiles induces single defects and also more complex defect aggregates. The evolution of the electron center concentration significantly depends on the beam parameters such as dose, fluence, and energy loss.

First, we will discuss the low-fluence regime, characterized by the mean distance between ion trajectories being much larger than the track radius r_F in which the F centers are created. The interaction of defects with neighboring tracks is in this case neglected, and the spectroscopic measurements describe the properties of individual tracks. The optical spectra are dominated by the absorption of simple point defects such as F and F_2 centers, without a significant contribution of more complex F_n centers (with $n=3,4$). The

ratio between F_2 and F centers is around 0.03, similar to the irradiation with γ rays or fast electrons.

With increasing fluence, individual ion tracks start to overlap leading to saturation of n_F and simultaneously to a decrease of n_F^s . For all ion projectiles, the saturation value of n_F is within 30% around $3 \times 10^{16} \text{ cm}^{-2}$ ($\pm 30\%$). The F-center track radius r_F grows with the energy loss from $\sim 2 \text{ nm}$ for He ions up to $\sim 18 \text{ nm}$ for Pb projectiles. Although this radius value is deduced with a simplified model (ignoring the inhomogeneous dose distribution around the ion path) it explains why the track overlapping phenomena occur for light projectiles at higher fluences than for heavy ions.

When tracks start to overlap, the aggregation of single F centers forming F_n and nF centers becomes more and more dominant. This effect is evident by the increase of defect clusters per track as in the initial high fluence stage. At even higher fluences, a^s reaches a maximum, and finally drops off at highest fluences (similar to the evolution of n_F^s). Whenever an additional projectile hits a preirradiated region, the recombination of primary hole centers (characterized by their high mobility) with F or F_n centers is efficient. The total concentration of all electron centers in the saturation region according to Eq. (8) for all ions is around $4\text{--}5 \times 10^{19} \text{ cm}^{-3}$. Because electron and hole centers always appear in pairs, the total defect concentration is as large as $\sim 8\text{--}10 \times 10^{19} \text{ cm}^{-3}$. This leads to a mean distance between individual defect centers of around 4 nm (~ 14 interatomic distances). Due to the nonuniform dose deposition, the real distance between electron and hole centers close to the ion trajectory is probably even smaller. From low-temperature experiments with KCl crystals,³⁰ it is known that stable F and H centers have a spacing of 4–5 interatomic distances, whereas at smaller distances, complete recombination can occur via tunneling processes.^{15,16,20}

The dominance of recombination and aggregation processes is also reflected in the F-center efficiency, which is only for light ions comparable to γ rays. In the nonoverlapping fluence regime, we interpret the lower efficiency of heavy projectiles as a direct signature of instantaneous recombination of primary Frenkel pairs as well as recombination of mobile primary hole centers with electron color centers in each track.^{16,17,20} These processes occur predominantly close to the ion path where the density of Frenkel pairs is high and the short distance between individual defects facilitates recombination and aggregation. The decrease of the F-center creation efficiency at higher fluences (e.g., for Pb ions: at high fluence $\Delta E_e = 3.5 \text{ keV}$ compared to $\Delta E_F \sim 1 \text{ keV}$ at low fluence) can also be ascribed to more pronounced recombination and aggregation processes taking additional place in overlapping track regions.

We finally address the problem of identification and quantification of defect complexes such as point defects (F_n centers), defect aggregates (nF centers), and metallic colloids. In particular at high fluences, the bands of the different F_n centers strongly overlap and therefore can not be quantified. The

broad absorption in the relevant wavelength region also makes the detection of small colloids impossible, which (according to classical radiation experiments) should form when a larger aggregate of halogen vacancies “collapses” to a metallic alkali complex. In principle, colloid identification in LiF can be performed by electron spin resonance (ESR). However, several ESR tests did not reveal any clear signal.¹⁵ Assuming that colloid formation occurs exclusively in the high-dose zone of the track core, we expect that the colloid size and concentration is extremely small and probably below the ESR sensitivity. In the track-overlapping regime, we can identify the 225-nm band that was already earlier assigned to more extended nF aggregates and which does not appear for single tracks. It should be mentioned that in annealing experiments using high-fluence samples, there was another band identified at 275 nm, which is also attributed to defect aggregation in overlapping track regions¹³.

V. CONCLUSIONS

Optical spectroscopy of color centers created in LiF crystals under room-temperature irradiation with MeV-GeV ions shows several characteristic phenomena. In the low-fluence regime, single ion tracks are well separated and the damage process is dominated by the formation of simple color centers such as F and F_2 centers. For heavy ion ($> \text{Xe}$), the efficiency for the creation of stable F centers is $\sim 1 \text{ keV}$, which is about a factor of 2 lower than for light ions ($\leq \text{C}$) and γ rays. The energy density in ion tracks produced at high stopping power is larger, and consequently the defect concentration increases significantly. At higher defect densities, the distance between single defects is smaller facilitating aggregation of individual electron (or hole) centers to defect clusters and also defect annihilation by recombination of hole and electron centers. The latter process determines the limited efficiency of color-center creation under heavy-ion irradiation.

At larger fluences where individual tracks overlap, the total F-center concentration saturates as a function of ion fluence, and thus the number of F centers per track decreases. The formation of defect aggregates becomes more and more important and clearly depends on the stopping power of the ions. The number of aggregates per track of heavy projectiles is up to two orders of magnitude larger than for light ions. It increases with fluence and finally surpasses a maximum, similar as the single defects.

ACKNOWLEDGMENTS

The irradiations with ^4He ions by H. Baumann (University of Frankfurt) are gratefully acknowledged. We also thank Ch. Lushchik and A. Lushchik (University of Tartu), E. Kotomin (MPI, Stuttgart and Latvian University, Riga), and M. Lang (GSI) for fruitful discussions. Access to irradiation experiments for M.T. was supported by the European Commission under the grant EC-HPRI-CT-1999-00001.

*FAX.: -49-6159-712179 Electronic address: c.trautmann@gsi.de

- ¹R. Kelly and H. M. Naguib, *Radiat. Eff.* **25**, 1 (1975).
- ²D. A. Young, *Nature (London)* **183**, 375 (1958).
- ³A. Perez, J. Davenas, and C. H. S. Dupuy, *Nucl. Instrum. Methods* **132**, 219 (1976).
- ⁴A. Perez, E. Balanzat, and J. Dural, *Phys. Rev. B* **41**, 3943 (1990).
- ⁵P. Thévenard, G. Guiraud, and C. H. S. Dupuy, *Radiat. Eff.* **32**, 89 (1977).
- ⁶E. Balanzat, S. Bouffard, A. Cassimi, E. Dooryhée, L. Protin, J. P. Grandin, J. L. Doualan, and J. Margerie, *Nucl. Instrum. Methods Phys. Res. B* **91**, 134 (1994).
- ⁷C. Trautmann, M. Toulemonde, J. M. Costantini, J. J. Grob, and K. Schwartz, *Phys. Rev. B* **62**, 13 (2001).
- ⁸A. Müller, R. Neumann, K. Schwartz, and C. Trautmann, *Nucl. Instrum. Methods Phys. Res. B* **146**, 393 (1998).
- ⁹C. Müller, M. Cranney, A. El-Said, N. Ishikawa, A. Iwase, M. Lang, and R. Neumann, *Nucl. Instrum. Methods Phys. Res. B* **191**, 246 (2002).
- ¹⁰M. Toulemonde, W. Assmann, C. Trautmann, and F. Grüner, *Phys. Rev. Lett.* **88**, 057602 (2002).
- ¹¹C. Trautmann, K. Schwartz, and O. Geiss, *J. Appl. Phys.* **83**, 3560 (1998).
- ¹²K. Schwartz, C. Trautmann, T. Steckenreiter, O. Geiß, and M. Krämer, *Phys. Rev. B* **58**, 11232 (1998).
- ¹³A. T. Davidson, K. Schwartz, J. D. Comins, A. G. Kozakiewicz, M. Toulemonde, and C. Trautmann, *Phys. Rev. B* **66**, 214102 (2002).
- ¹⁴K. Schwartz, G. Wirth, C. Trautmann, and T. Steckenreiter, *Phys. Rev. B* **56**, 10 711 (1997).
- ¹⁵C. Trautmann, M. Toulemonde, K. Schwartz, J. M. Costantini, and A. Müller, *Nucl. Instrum. Methods Phys. Res. B* **164/165**, 365 (2000).
- ¹⁶N. Itoh and M. Stoneham, *Materials Modification by Electronic Excitation* (Cambridge University Press, Cambridge, 2001).
- ¹⁷Ch. B. Lushchik, in *Physics of Radiation Effects in Crystals*, edited by R. A. Johnson and A. N. Orlov (North-Holland, Amsterdam, 1986), pp. 473.
- ¹⁸M. R. Mayhugh and R. W. Christy, *Phys. Rev. B* **2**, 3330 (1970).
- ¹⁹M. R. Mayhugh, *J. Appl. Phys.* **41**, 4776 (1970).
- ²⁰Ch. B. Lushchik, I. K. Vitol, and A. Elango, *Sov. Phys. Usp.* **20**, 489 (1977).
- ²¹Ch. B. Lushchik, G. G. Lydia, and M. A. Elango, *Sov. Phys. Solid State* **6**, 1789 (1965).
- ²²Yu. M. Alexandrov, Ch. B. Lushchik, V. N. Makhov, T. I. Sireishchikov, and M. N. akhimenko, *Sov. Phys. Solid State* **24**, 968 (1982).
- ²³B. P. Aduyev and D. I. Vaisburd, *Sov. Phys. Solid State* **23**, 1869 (1981).
- ²⁴A. Lushchik, M. Kirm, Ch. Lushchik, and E. Vasil'chenko, *Nucl. Instrum. Methods Phys. Res. B* **166-167**, 529 (2000).
- ²⁵A. E. Hughes and S. C. Jain, *Adv. Phys.* **28**, 717 (1979).
- ²⁶J. F. Ziegler, J. P. Biersack, and U. Littmark, in *The Stopping and Ranges of Ions in Solids*, edited by J. F. Ziegler (Pergamon, New York, 1985).
- ²⁷R. L. Fleischer, P. B. Price, and R. M. Walker, *Nuclear Tracks in Solids: Principles and Applications* (University of California, Berkeley, 1975).
- ²⁸P. Thévenard, G. Guiraud, C. H. S. Dupuy, and B. Delaunay, *Radiat. Eff.* **32**, 83 (1977).
- ²⁹Ch. J. Delbecq and P. Pringsheim, *J. Chem. Phys.* **21**, 794 (1953).
- ³⁰A. Ch. Lushchik and Ch. B. Lushchik, *Bull. Acad. Sci. USSR, Phys. Ser. (Engl. Transl.)* **56**, 201 (1992).
- ³¹J. H. Crawford, *Adv. Phys.* **17**, 93 (1968).
- ³²H. Rabin and C. Klick, *Phys. Rev.* **117**, 1005 (1960).
- ³³P. W. Levy, *J. Phys. Chem. Solids* **52**, 319 (1991).
- ³⁴G. A. Russell and C. Klick, *Phys. Rev.* **101**, 1473 (1956).